Applied Catalysis B: Environment and Energy 345 (2024) 123718

Contents lists available at ScienceDirect

Applied Catalysis B: Environment and Energy

journal homepage: www.elsevier.com/locate/apcatb

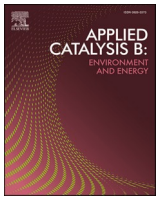

Sustainable microwave-driven CO_2 gasification of plastic waste for high-yield H_2 and CO production

Peng Zhang, Cai Liang *, Mudi Wu *, Yongjie Li, Xiaoping Chen, Daoyin Liu, Jiliang Ma

Key Laboratory of Energy Thermal Conversion and Control of Ministry of Education, School of Energy and Environment, Southeast University, Nanjing 211189, China

ARTICLE INFO

Keywords:
Plastic waste
CO_2 gasification
Microwave
Hydrogen
Sustainability

ABSTRACT

The efficiency and sustainability for the recycling of plastic wastes into hydrogen was investigated. An integrated microwave-driven valorization of plastic wastes and CO_2 for H_2 and CO production was proposed. Specifically, plastic wastes were decomposed into H_2 and solid carbons, followed by carbon elimination via CO_2 gasification under microwave irradiation. Through the high-throughput screen of catalysts as well as the optimization of key parameters, over 96% hydrogen was converted into H_2 with a yield of 480 mmol•$g^{-1}H_{plastic}$ while the carbon conversion and CO_2 conversion reached up to 70% and 53%. The five-cycle successive test displayed extraordinarily high and stable catalytic activity due to the facile elimination of carbon deposition. The application for real-world plastic wastes further demonstrated the efficient microwave-driven CO_2 gasification of plastic wastes into H_2 and CO production as a feasible and sustainable technology toward the waste-to-energy circular economy.

1. Introduction

With the worldwide commitment to tackling environmental pollution, climate crisis and carbon emission, the demand for clean energy and waste valorization is on the rise [1,2]. The manufacture of plastic products has been booming with myriad applications across the whole world, but the management of plastic wastes poses an enormous threat [3]. It is imperative to explore efficient strategies for the recycling of plastic wastes into valuable fuels and chemicals in view of sustainable development and environmental pollution treatment [4–6]. However, the current plastic recycling technologies often entail the release of greenhouse gas CO_2. Facilitating the mitigation of CO_2 emission and the CO_2 utilization into value-added products are crucial for achieving a carbon circular economy [7–9]. Given this, an integrated strategy for efficient and sustainable valorization of plastic wastes and CO_2 is promising and attractive, but challenging [10,11].

Over the past decades, various methods have been developed to convert plastic wastes into hydrogen [12,13], hydrocarbons (HCs) [14,15], syngas [16,17] and solid carbon materials [18,19]. It is noteworthy that the two-step chemical process via pyrolysis [20–22] and reforming process [21,23] has been proven to be effective in enhancing conversion efficiency and product selectivity [24,25]. The plastic wastes were firstly converted into small-chained HCs vapers, followed by catalytic reforming for hydrogen-rich production. However, the two-step method suffered from inherent drawbacks including high energy input, complicated processing flow and inevitable CO_2 emission [26–28]. To overcome these limitations, a one-step microwave-initiated deconstruction method [27,29] coupled with highly efficient microwave catalysts [22,30] has been proposed and advanced. This alternative enabled the rapid and selective initiation of the decomposition process by utilizing the interactions of the microwave-susceptor materials with the electromagnetic field instead of heating the whole reaction system [31–33]. Under microwave irradiation, hydrogen products with extremely high efficiency were generated, leaving abundant solid carbons. Nevertheless, those carbons deposited on the catalyst surface would dramatically impede the catalytical performance by hindering the contact between reactants and active sites. It has been reported that the yield of H_2 decreased to less than one-third of the first cycle in the cycle test accompanied with accumulated carbon deposition [27]. The conventional avenue to separate solid carbons from catalysts was acid treatment, which unfortunately led to irreversible damage to the catalysts [34,35]. Thus, it is crucial to propose innovative strategies to ensure high and stable hydrogen production from the perspective of large-scale practical utilization for economy and sustainability.

Introducing CO_2 into the decomposition process has been considered as a feasible approach since CO_2 could participate in the reforming of

* Corresponding authors.
E-mail addresses: liangc@seu.edu.cn (C. Liang), wumudi@outlook.com (M. Wu).

https://doi.org/10.1016/j.apcatb.2024.123718
Received 14 September 2023; Received in revised form 2 January 2024; Accepted 7 January 2024
Available online 11 January 2024

Table 1
Ultimate analysis of the plastics used in this work.

Sample	Ultimate analysis (wt%)		
	C	H	O
PE powder	84.97	12.52	2.26
Plastic bag	82.96	12.53	3.60
Plastic wrap	84.53	12.94	0.86
Medical mask	84.88	13.31	1.76
KN95 mask	83.72	12.78	2.36
Plastic bottle	62.11	4.05	33.42

short-chained HCs [36] or facilitate the removal of deposited carbon [37]. Distinct from the inevitable CO_2 emission in traditional thermochemical technology, such a method could in turn consume and convert CO_2 into value-added products. In recent studies, the utilization of H_2O [16,21] and CO_2 [38] as gasification agents has been reported in the conversion of food wastes [39], sludge [40], plastics [41,42] and so on. The CO_2-mediated treatment of several plastic wastes has been investigated through a multi-stage furnace system [43,44]. Traditional supported catalysts such as Ni/SiO_2 and Co/SiO_2 were employed to enhance H_2 formation. It was observed that CO_2, acting as a co-reactant at high temperatures, could promote the conversion of HCs into H_2 and CO and inhibit the undesired coke deposition. However, the high temperature was required (e.g., over 700 °C) to facilitate the activation of CO_2 for gasification during the reaction process. In the traditional CO_2 gasification method, tremendous amount of energy input was needed for the low efficiency of heating the whole reaction region. Considering that microwave could activate the CO_2 at a relatively low temperature by changing thermodynamics with dropped apparent activation energy [37], the microwave-driven CO_2 gasification should be a efficient method for plastic recycling with less energy input and time cost. From the perspective of catalysts, conventional catalysts were not suitable for the microwave-driven system due to the poor microwave absorption properties of supports like SiO_2 and TiO_2. The design of microwave-catalyst design was considerably more intricate and needed to fulfill a triple role: (1) functioning as the catalyst, (2) serving as the microwave absorber, and (3) acting as the carbon dioxide adsorbent. In this regard, a high-throughput screen of metal catalysts should be necessary. Moreover, CO_2 needed to be activated at high temperatures to participate into the decomposition process, which further requires optimization of microwave parameters as well as the catalysts [45,46]. Quantitative analysis of operation parameters for the microwave CO_2-reforming of polyethylene without catalysts has been evaluated [40,47]. Increasing pyrolysis temperature and introducing CO_2 were reported to change the carbon reallocation ability of polyethylene, with the carbon mainly migrating from the oil to gas production. However, the yield of H_2 was low and HCs still accounted for a wide share. To the best of our knowledge, few studies have focused on the microwave-driven catalytic CO_2 gasification of plastic wastes into H_2 and CO.

At present, the efficiency and sustainability of converting plastic wastes into high yield H_2 and CO production are in a reconciled dilemma. The conventional thermal-reforming methods suffered from high energy consumption and low efficiency while the microwave-initiated decomposition of plastics was restricted by demanding catalysts and low sustainability. Herein, we proposed a microwave-driven catalytic CO_2 gasification system for sustainable and efficient valorization of real-world plastic wastes for high-yield H_2 and CO production. A high-throughput screen of transition metal oxide catalysts was conducted, where the H_2 yield and carbon conversion were employed to evaluate the catalytic performance. The parameters of the microwave-driven process were optimized via the response surface analysis. Furthermore, the reaction pathway of CO_2 involved in the decomposition of plastics as well as the removal of carbon deposition has not been unrevealed. To provide intrinsic insight into the reaction process, the elaboration of plastic dissociation and carbon evolution was proposed by time-on-stream gas analysis and mimicked in-situ characterization. The comparison test between the thermal process and microwave process highlighted the facile activation of CO_2 gasification agent under microwaves while the successive cycle test exhibited the sustainability for H_2 and CO production. In addition, five typical plastic wastes in our daily life were employed as feedstocks to assess the potential for practical applications. Generally, the microwave-driven valorization system provided an efficient and sustainable alternative to convert plastic wastes into H_2 and CO via CO_2 gasification, which benefited the circular economy.

2. Experimental

2.1. Materials and catalyst preparation

The low-density polyethylene (PE) powder and five kinds of real-world plastic wastes (plastic bags, plastic wraps, medical masks, KN95 masks and plastic bottles) were employed for experiments. The PE powder purchased from the local factory was in the size of 24–30 mesh while the real-world plastic wastes collected from stores were cut into small pieces (less than 3 mm). The ultimate analysis of these plastics was determined by an Elementar Vario EL as shown in Table 1.

All the chemicals in this work were used as received without further purification. Iron nitrate nonahydrate ($Fe(NO_3)_3{\cdot}9\ H_2O$, 99%), nickel nitrate hexahydrate ($Ni(NO_3)_2{\cdot}6\ H_2O$, 99%), cobalt nitrate hexahydrate ($Co(NO_3)_2{\cdot}6\ H_2O$, 99%), aluminum nitrate nonahydrate ($Al(NO_3)_3{\cdot}9\ H_2O$, 99%), lanthanum nitrate hexahydrate ($La(NO_3)_3{\cdot}6\ H_2O$, 99%), magnesium nitrate hexahydrate ($Mg(NO_3)_2{\cdot}6\ H_2O$, 99%), calcium nitrate tetrahydrate ($Ca(NO_3)_2{\cdot}4\ H_2O$, 99%), citric acid ($C_6H_8O_7{\cdot}4\ H_2O$, 99.8%) and ethylene glycol ($C_2H_6O_2$, 99.5%) were obtained from Sino pharm. Four kinds of carbon materials including activated carbon (AC), carbon black (CB), graphite (GC) and carbon nanotube (CNT) were purchased from Aladdin.

The metal oxide catalysts were synthesized via the Pechini method. Briefly, stoichiometric amounts of metal nitrates (La/Mg/Ca/Al: Fe/NiCo = 1:1) were dissolved into deionized water under stirring until the complete solution. Citric acid and ethylene glycol with a molar ratio of 1:2:1 to the metal nitrates were added to the solution individually. Then the mixture was evaporated at 80 °C until a viscous gel was formed, and the gel was dried in the oven at 110 °C for 24 h. Subsequently, the dry gel was calcined at 800 °C for 3 h with a temperature ramp of 5 °C·min^{-1}. The catalysts were ground and sieved into the same size range. The catalysts were named as ABO_x based on the metal nitrates (A= La, Mg, Ca and Al, B = Fe, Ni and Co).

2.2. Experimental setup and procedure

Microwave decomposition of plastic wastes was conducted using a custom-built single-mode microwave reaction system (Fig. 1). As shown in Fig. 1a, the microwave reaction system consisted of a microwave generator and control system, a microwave circulator, a water load, a bent waveguide, 3-stub tuners, a custom-built microwave cavity and a movable plunger. The operation frequency was 2.45 GHz, and the output power could be adjusted from 0 to 1000 W continuously. The transverse electric (TE) mode was TE_{10}. The reaction cavity was designed to irradiate the catalysts and initiate the decomposition of plastics, and the details of the cavity were illustrated in Fig. 1b. Given that the plastics would melt during the microwave irradiation process, such a semi-open quartz tube reactor was adopted other than the common pass-through quartz tube (inner diameter: 12 mm, height: 200 mm). The melted plastics would remain in the bottle of the quartz tube without leaking, and therefore the complete decomposition of waste plastics was guaranteed. Typically, 0.3 g catalysts and 0.3 g plastics were mixed and then placed on the bottom of the semi-open quartz tube. The quartz tube was then placed at the center of the microwave cavity to

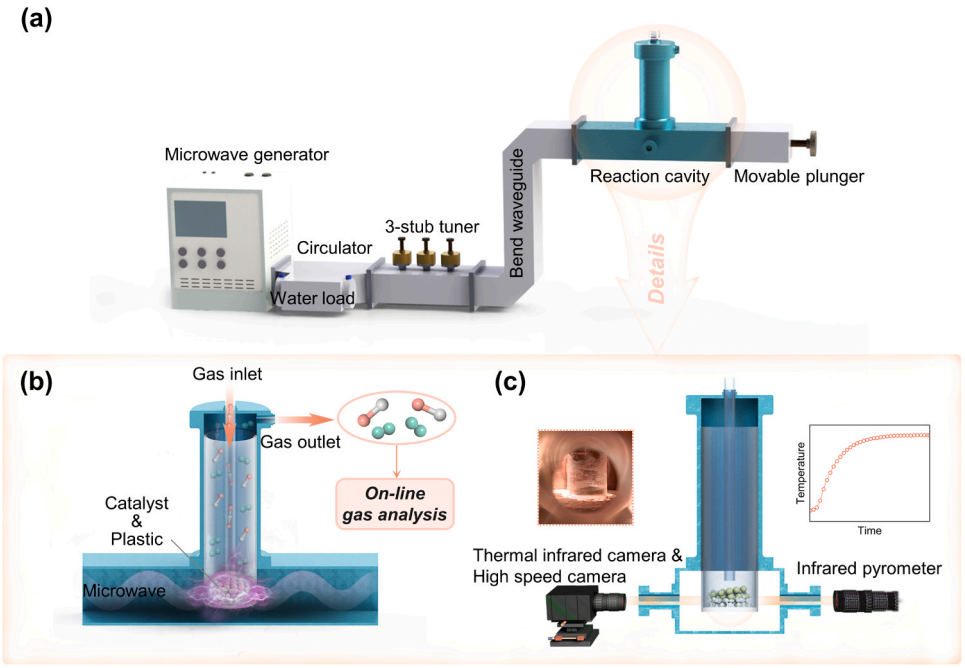

Fig. 1. Schematic diagram of microwave reaction system. (a) Microwave reaction system; (b) Details of microwave reaction cavity; (c) Configuration of the simultaneous measurement system. The infrared pyrometer, thermal infrared camera and high-speed camera was placed at the side of the reaction cavity.

ensure uniform microwave irradiation. The inlet gas controlled by a mass flow controller was from the top inlet of the quartz tube, passed through the mixed samples, and then flowed out from the lateral outlet. The flow rate of inlet gas was set as 200 ml/min. The whole sealed system was purged with the N_2 flow of 200 ml•min^{-1} for 20 min to eliminate the residual air. The evolved gases would be analyzed in real time by the gas analyzer coupled with thermal conductivity detector and non-dispersive infrared detector (MRU Vario Plus New). The simultaneous temperature was recorded by an infrared pyrometer (Optris CT LT) with a temperature range from 0–975 °C and the dynamic feature of mixed samples under irradiation was captured by a thermal infrared camera (Magnity technologies MAG91) and a high-speed camera (FASTCAM SA4). The configuration of these measurements was shown in Fig. 1c.

For comparison, the thermal-driven experiment was conducted in a tubular furnace (OTL1200, NANDA instrument). The system was shown in Fig. S1. 0.3 g catalysts and 0.3 g plastics were mixed in a quartz ark and then put into the center of the heating zone. Similarly, the whole system was purged with the N_2 flow of 200 ml•min^{-1} for 20 min to eliminate the residual air. The temperature was set to increase from 30 °C to 500 °C/700 °C with a fixed heating rate of 10 °C•min^{-1}. The other procedures were the same as the microwave-driven experiment.

2.3. Performance evaluation

The real-time flow rate of evolved gases was analyzed by the gas analyzer (MRU Vario Plus New) and the cumulative volume of the evolved gases was integrated from the flow rate by applying N_2 as internal standard. The flow rate and cumulative volume of each gas in real-time are calculated as

$$\text{Flow rate}_i\ (\text{ml}\cdot\text{min}^{-1}) = \text{Flow rate}_{N_2} \times \frac{C_i}{C_{N_2}} \quad (1)$$

$$\text{Cumulative volume}_i\ (\text{ml}) = \int_0^t \text{Flow rate}_i\ dt \quad (2)$$

where C_i represented the volume fraction of the evolved gases obtained from the gas analyzer.

The composition of the evolved gases was calculated from the cumulative volume. For comparison, the evolved gases over selected catalysts were collected and analyzed by gas chromatography (GC, Agilent 7890 A, Thermo, USA). Thermal conductivity detector (TCD) was employed to detect the concentration of H_2, CO_2, N_2, O_2, and CO, and the column was HP-PLOT/Q (30 m × 0.32 mm×20 μm). Flame ionization detector (FID) was used to detect hydrocarbon gases (CH_4, C_2H_4, C_2H_6, C_3H_8, C_3H_6), and the column was HP-PLOT/Q (30 m × 0.32 mm×20 μm).

The yield of H_2 was defined as

$$H_2\ \text{yield}\ (\text{mmol}\cdot\text{g}^{-1}H_{\text{plastic}}) = \frac{\text{Mole}_{H_2}}{\text{Mass}^{H}_{\text{plastic}}} \quad (3)$$

The efficiency of hydrogen was determined as

$$\text{Hydrogen efficiency}\ (\%) = \frac{\text{Mass}^{H}_{H_2} + \text{Mass}^{H}_{CH_4}}{\text{Mass}^{H}_{\text{plastic}}} \quad (4)$$

Where Mole_{H_2} was the moles of the generated H_2, and $\text{Mass}^{H}_{\text{plastic}}$,$\text{Mass}^{H}_{CH}4$, $\text{Mass}^{H}_{H_2}$ were the theoretical mass of hydrogen in the consumed plastics and the mass of hydrogen in H_2 and CH_4 for each experiment.

The conversion of carbon was calculated as

$$\text{Carbon conversion}\ (\%) = \frac{\text{Mass}^{C}_{CO}}{2 \times \text{Mass}^{C}_{\text{plastic}}} \quad (5)$$

Where Mass^{C}_{CO} was the mass of carbon element in the generated CO products and $\text{Mass}^{C}_{\text{plastic}}$ was the mass of carbon elements in the consumed plastics.

The conversion of CO_2 was calculated as

$$CO_2\ \text{conversion}\ (\%) = \frac{V_{CO_2,in} - V_{CO_2,out}}{V_{CO_2,in}} \quad (6)$$

Where $V_{CO_2,in}$ and $V_{CO_2,out}$ refer to the CO_2 volume of inlet and outlet during the reaction time.

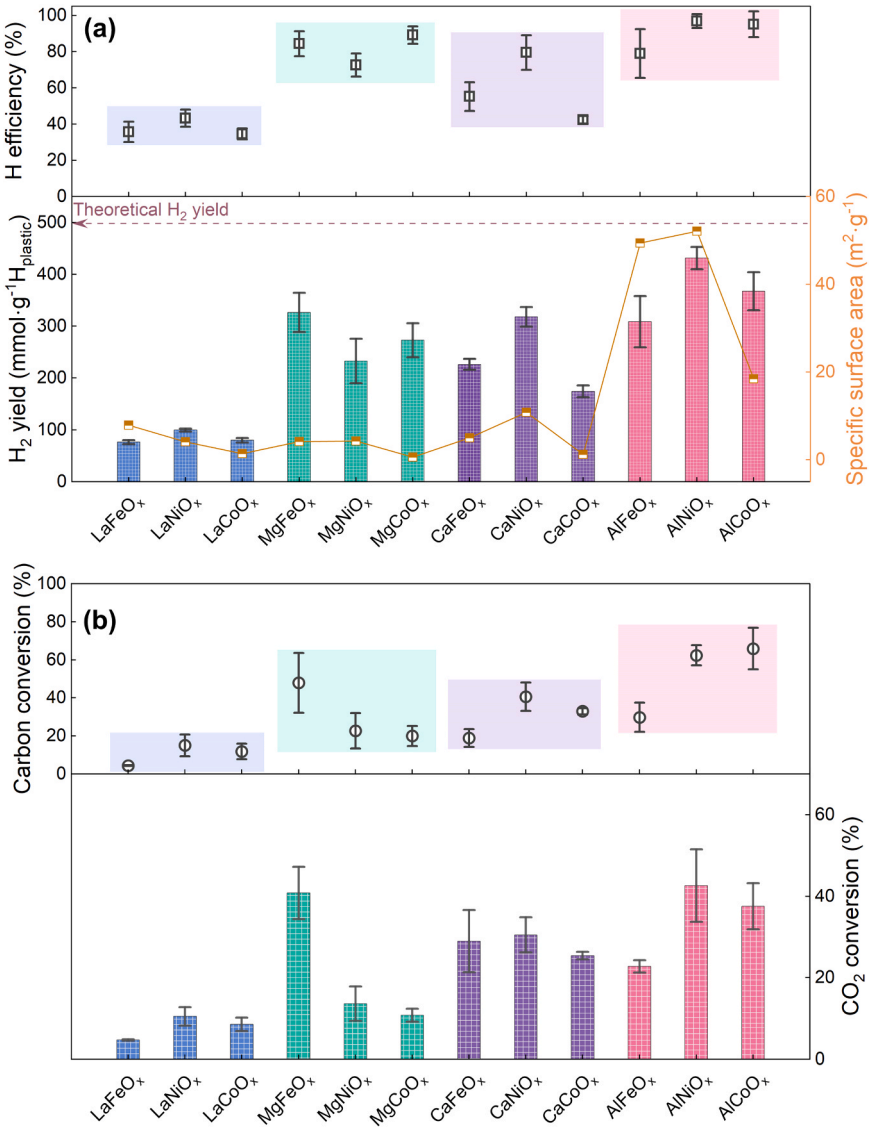

Fig. 2. Performance of the valorization of 0.3 g PE with 50 vol% CO_2 using 0.3 g tested transition metal oxide catalysts. (a) Hydrogen efficiency and H_2 yield with relationship to the catalyst specific surface area; (b) Carbon conversion and CO_2 conversion.

2.4. Characterization

The X-ray diffraction (XRD) patterns were recorded on a Rigaku Smartlab X-ray diffractometer in the range from 10° to 80° (2θ) with a scanning rate of 5°·min^{-1}. The average crystallite size of metal particles was calculated by the Scherrer equation. The specific surface area was calculated by the Brunauer-Emmet-Teller (BET) method and the pore size distribution was calculated by the Barret-Joyner-Halenda (BJH) method from the desorption branches of the isotherms through the nitrogen adsorption-desorption analyzer (Micromeritics ASAP 2460). The Fourier transform infrared spectroscopy (FT-IR) was detected on a Nicolet iS50 spectrometer. The thermogravimetric analysis (TGA) was conducted on a TG209 F3 thermal analyzer for the residual solid carbon over the catalysts. Before the test, 20 mg samples were pretreated by Ar at 200 °C for 1 h and cooled down to 50 °C. After that, the temperature was increased from RT to 800 °C with a heating rate of 10 °C•min^{-1}. The Scanning electron microscopic (SEM) images were taken with a Quanta 400 FEG. The TEM images were recorded on an FEI Talos F200S field-emission transmission electron microscope at an acceleration voltage of 200 kV. Energy dispersive X-ray (EDX) mapping was performed to further visualize the morphologies of the samples. Raman spectrometer (Renishaw inVia) equipped with a wavelength of 532 nm was used for the characterization of carbon products. X-ray photoelectron spectroscopy (XPS, Thermo Escalab 250Xi) was employed to determine the chemical state of the catalysts. The microwave absorbing performance of the catalysts was measured by the Vector Network Analyzer (Agilent E5071C).

3. Results and discussion

3.1. High-throughput screen of transition metal oxide catalysts

The microwave-driven decomposition of PE powder and CO_2 was conducted over a series of transition metal oxide catalysts for at least three times per catalyst. The typical gas composition and temperature curve in real-time were shown in Figs. S2–5. The H_2 yield exhibited a marked variability for different A elements, giving less than 100 mmol•g$^{-1}H_{plastic}$ for $LaBO_x$, 100–300 mmol•g$^{-1}H_{plastic}$ for $MgBO_x$ and $CaBO_x$, and over 300 mmol•g$^{-1}H_{plastic}$ for $AlBO_x$ (Fig. 2a). Notably, the H_2 yield of $AlNiO_x$ reached up to 450 mmol•g$^{-1}H_{plastic}$, which was over 90% of the theoretical value. This suggested a potential avenue to convert the whole hydrogen elements into H_2 in the future.

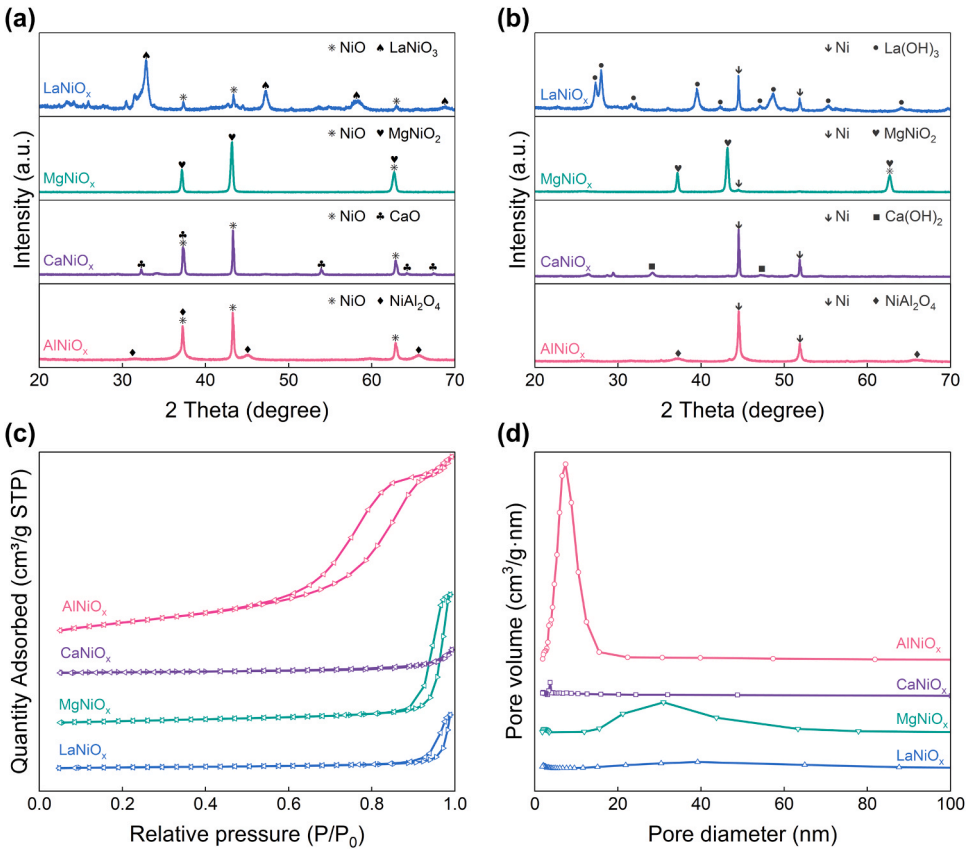

Fig. 3. Characterization of $ANiO_x$ (A = La, Mg, Ca and Al) catalysts. (a) X-ray diffraction patterns of fresh catalysts; (b) X-ray diffraction patterns of spent catalysts; (c) N_2 adsorption-desorption isothermals curves and (d) corresponding pore size distribution of the fresh catalysts.

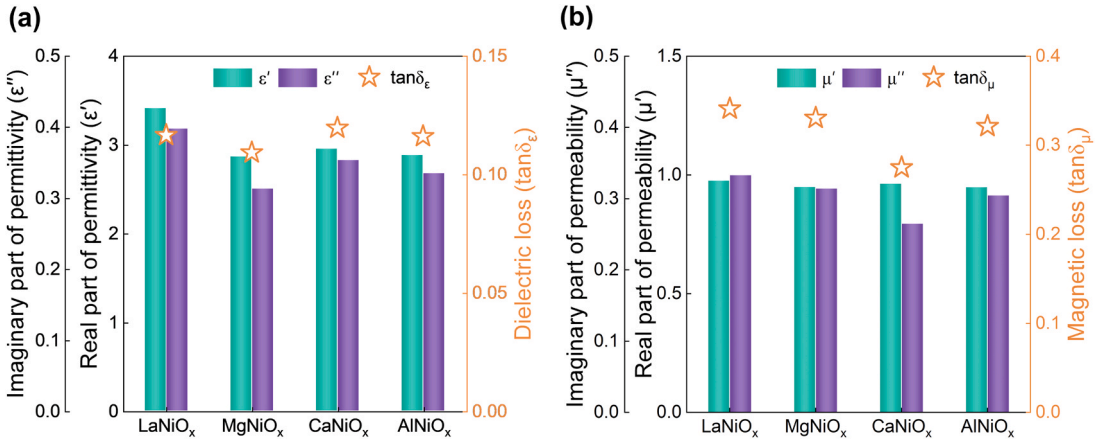

Fig. 4. Electromagnetic parameters of the fresh catalysts. (a) Permittivity and dielectric loss; (b) Permeability and magnetic loss.

Correspondingly, the hydrogen efficiency which includes the H_2 and CH_4 was calculated. Similarly, the hydrogen efficiency of $LaBO_x$ was less than 50%, indicating the preferred generation of short-chained HCs owing to the insufficient decomposition of plastics. This phenomenon was in agreement with the results from GC in Fig. S6 that HCs (C_2H_4, C_2H_6 and C_3H_6) accounted for over 15 vol%. The highest hydrogen efficiency for $AlBO_x$ was over 80% (80% $AlFeO_x$, 98% $AlNiO_x$, 92% $AlCoO_x$). The gas composition evaluated from GC over $AlNiO_x$ also demonstrated that the plastics were completely converted into H_2, CO and extremely few CH_4 without other HCs. The carbon conversion and CO_2 conversion were further analyzed and the results were shown in Fig. 2b. For $LaBO_x$, the carbon conversion (< 20%) and CO_2 conversion (< 10%) were both relatively low, which suggested that the majority of CO_2 gas was not activated and acted only as the carrier gas instead of the reactant gas. Similar to the trend of H_2 yield, $AlBO_x$ exhibited the highest carbon conversion, followed by $CaBO_x$ and $MgBO_x$. In general, the H_2 yield and carbon conversion basically maintained the same pattern. $AlNiO_x$ catalysts were proved to be the most effective in terms of conversion of plastics into H_2 and CO.

The specific surface area of all the catalysts were measured and shown in Fig. 2. Results showed that the specific surface area varied from 1 $m^2 \bullet g^{-1}$ to 60 $m^2 \bullet g^{-1}$ among the as-prepared catalysts and directly related to the catalytic activity. In detail, the specific surface area of $AlBO_x$ catalysts were high ($AlFeO_x$: 49.44 $m^2 \bullet g^{-1}$, $AlNiO_x$:

Table 2
Physicochemical properties of the catalysts.

Catalyst	BET surface area (m^2/g)	Pore volume (cm^3/g)	Pore size (nm)	Crystallite size[a] (nm)	Ni^0 / (Ni^0 + Ni^{2+})[b]
$LaNiO_x$	4.09	0.018	16.43	29.60	0.568
$MgNiO_x$	4.31	0.040	33.64	14.07	0.019
$CaNiO_x$	10.81	0.097	30.7	34.17	0.253
$AlNiO_x$	52.13	0.144	8.09	31.65	0.139

[a] Obtained from XRD patterns of spent catalysts by Scherrer equation.
[b] Determined from XPS results of spent catalysts.

52.13 $m^2 \bullet g^{-1}$, $AlCoO_x$: 18.49 $m^2 \bullet g^{-1}$) while the specific surface area of other catalysts were less than 10 $m^2 \bullet g^{-1}$. In the heterogeneous catalytic process, the contact between catalysts and reactants was influenced by the dispersion and number of active sites. More active sites would be fabricated from the in-situ exsolution process over the catalysts with a high specific surface area. Therefore, the highest H_2 yield and carbon conversion were achieved over the $AlNiO_x$ with the highest specific surface area.

To reveal the significant difference in catalytical performance under microwave irradiation, four kinds of $ANiO_x$ (A = La, Mg, Ca and Al) were further characterized (Fig. 3, Fig. 4 and Fig. S7, Table 2). As shown in Fig. 3a, the peaks of NiO (PDF# 44–1159) at 37.25°, 43.29° and 62.85° assigned to the crystal plane (101), (012) and (110) were detected for all the fresh catalysts. For $MgNiO_x$, the dominant structure was the $MgNiO_2$ (PDF# 24–0712) with diffraction peaks at 37.10°, 43.10° and 62.60°. It should be noted that the strong intensity of $MgNiO_2$ reflected the high crystallinity and little impurities like NiO were detected, suggesting the majority of Ni was bonded with Mg to form a structurally stable system [48]. The dominant phase for the other three catalysts was NiO accompanied by $LaNiO_3$ (PDF# 34–1077), CaO (PDF# 77–2010) and $NiAl_2O_4$ (PDF# 78–1601), respectively. It could be speculated that more NiO other than those multi-metal oxides such as perovskite and spinel promote the exsolution of metallic Ni active sites due to the modest metal-support interaction [49].

This could be evidenced by the evolution of the crystalline phase before and after the reaction. The XRD patterns of spent catalysts after the 300 s experiment were detected in Fig. 3b. Strikingly, the crystalline phase of nickel experienced the in-situ transformation from the oxidized state into the metallic state along with the H_2 generation during the reaction. The diffraction peaks ascribed to metallic nickel (PDF#

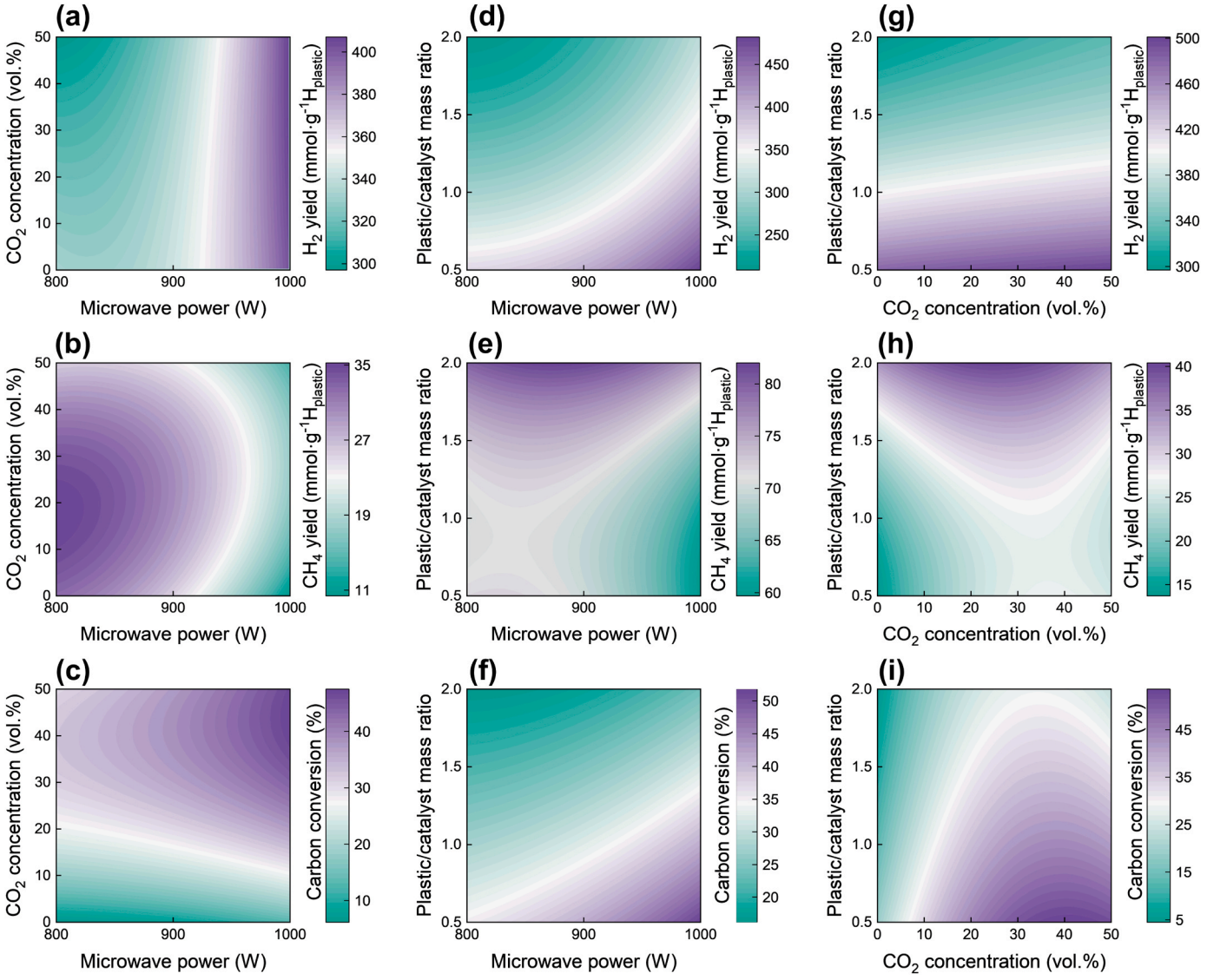

Fig. 5. Parametric study on the performance of microwave-driven valorization of plastic wastes and CO_2. (Microwave power: 800 W-1000 W; Plastic/catalyst mass ratio: 0.5–2; CO_2 concentration: 0 vol%−50 vol%).

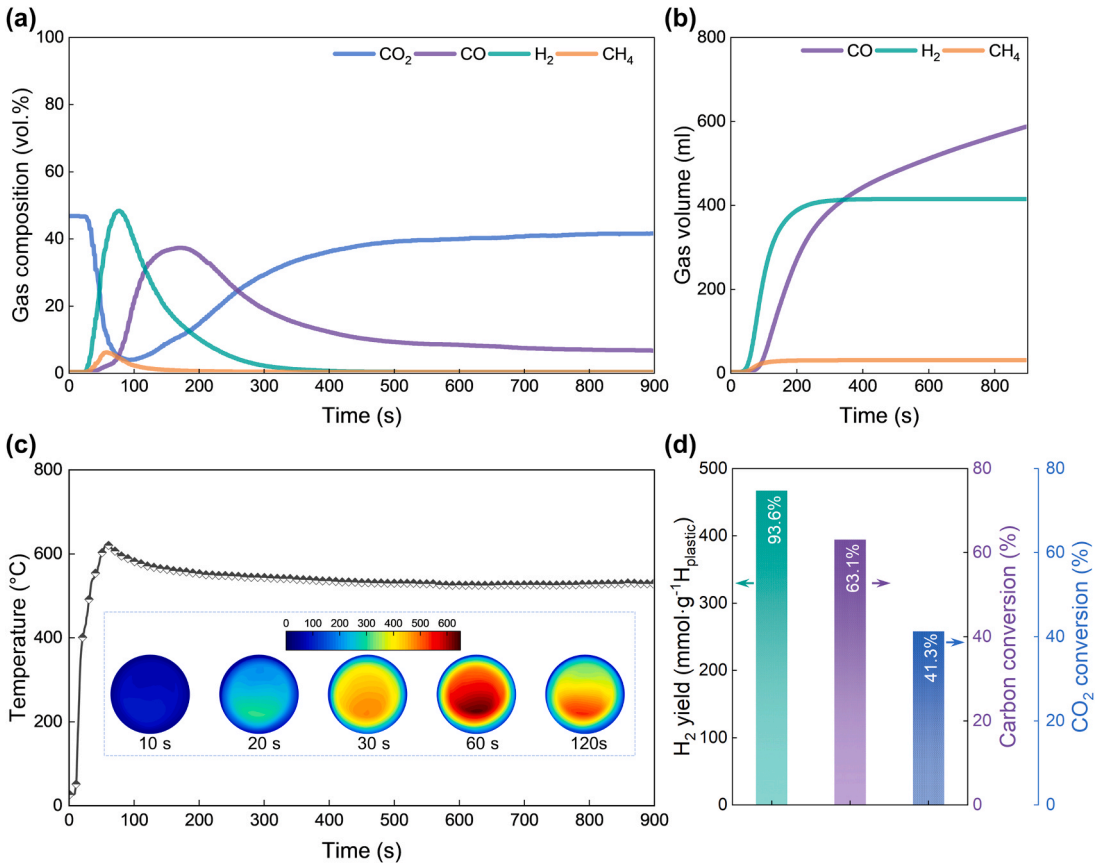

Fig. 6. Time-on-stream analysis of microwave-driven valorization of 0.3 g plastic wastes and CO_2 using 0.3 g $AlNiO_x$ catalyst. (a) Real-time gas composition of evolved gases and (b) corresponding accumulated gas volume; (c) Temperature profiles of the samples during the reaction process; (d) H_2 yield, carbon conversion and CO_2 conversion.

04–0850) were observed at 44.5° and 51.8°. The prominent phase of spent $LaNiO_x$, $CaNiO_x$ and $AlNiO_x$ were metallic Ni, suggesting the exsolution of metallic Ni from the crystal lattice and enrichment over the catalyst surface. This was beneficial for the catalytic performance since metallic nickel other than oxidized nickel was the active site. By contrast, the spent $MgNiO_x$ still retained the structure of $MgNiO_2$ and the intensity of metallic nickel was quite weak. This was attributed to the strong interaction between Ni and the substrate as mentioned before. Nickel elements were bonded with the crystal lattice and hard to exsolve out to the surface, which would inevitably result in the unsatisfied decomposition of plastic wastes. Moreover, the crystallite size of metallic nanoparticles was calculated according to the diffraction peak of the lowest 2θ value and the average size of Ni was around 14–31 nm without agglomeration or sintering (Table 2). For comparison, the XRD patterns of catalysts under thermal reduction of 5 vol% H_2 for 60 min were characterized (Fig. S7). Similarly, the metallic nickel phase was detected for the four kinds of catalysts. However, peaks of the NiO phase still existed with weaker intensity. This indicated that the reduction rate of thermal conditions was less efficient than in-situ microwave reduction. In fact, the microwave synthetic method has been applied in several aspects including nanoporous materials, metal-organic frameworks, covalent organic frameworks, metal oxides and carbonaceous materials due to the energy-efficient and time-saving features [50].

The N_2 adsorption-desorption isotherms as well as the pore size distribution curves of the corresponding catalysts were shown in Fig. 3c and d, and the surface area and pore information were tabulated in Table 2. All catalysts possessed the typical type IV isotherms with H3 hysteresis loops at the high-pressure range (P/P_0) of 0.6–1.0, suggesting the existence of mesoporous structure. The specific surface area of $LaNiO_x$, $MgNiO_x$ and $CaNiO_x$ were 4.09 $m^2 \bullet g^{-1}$, 4.31 $m^2 \bullet g^{-1}$ and 10.81 $m^2 \bullet g^{-1}$, respectively. In comparison, the specific surface area had a significant elevation and came up to 52.13 $m^2 \bullet g^{-1}$ for $AlNiO_x$, which would undoubtedly improve the catalytic activity. In addition, the pore volume showed the same trend that $AlNiO_x$ has the largest pore volume of 0.144 $cm^3 \bullet g^{-1}$. Conversely, the pore size distribution of $AlNiO_x$ was concentrated at 7.4 nm as shown in Fig. 3d with the average pore size of 8.09 nm. In all, compared with the $LaNiO_x$, $MgNiO_x$ and $CaNiO_x$, the $AlNiO_x$ possessed a higher specific surface area, larger pore volume and smaller pore size, which may promote the exsolution of active sites and the frequency for solid-solid contact.

To further elucidate the catalytic performance with regard to the accessible active sites, the valence information of surface Ni species was characterized by XPS analysis and the results were shown in Fig. S8 and Table 2. The Ni $2p_{3/2}$ spectra of four kinds of spent catalysts displayed three contributions involving Ni^0 (852.7 eV – 852.9 eV), Ni^{2+} (855.7 eV - 856.1 eV) and the satellite peak [38]. Therefore, metallic Ni and oxidized were co-existed in the spent catalysts and this was in agreement with the results from the XRD patterns. The ratio of Ni^0 / (Ni^0 + Ni^{2+}) was calculated and results showed that the value of $MgNiO_x$ was one order of magnitude smaller than the other three catalysts. More Ni species were in-situ reduced into metallic state for $AlNiO_x$, $LaNiO_x$ and $CaNiO_x$ while the majority of Ni species remained oxidation state for $MgNiO_x$. The specific surface area and the ratio of metallic Ni contributed to the dispersion of active sites cooperatively and further influenced the catalytic performance.

Catalysts played dual roles of the catalyst itself as well as the microwave susceptor simultaneously in the microwave-driven system. Thus, the microwave absorption performance including the complex permittivity ($\varepsilon = \varepsilon' - j\varepsilon''$) and complex permeability ($\mu = \mu' - j\mu''$) was evaluated via the coaxial method at room temperature [51]. The real part

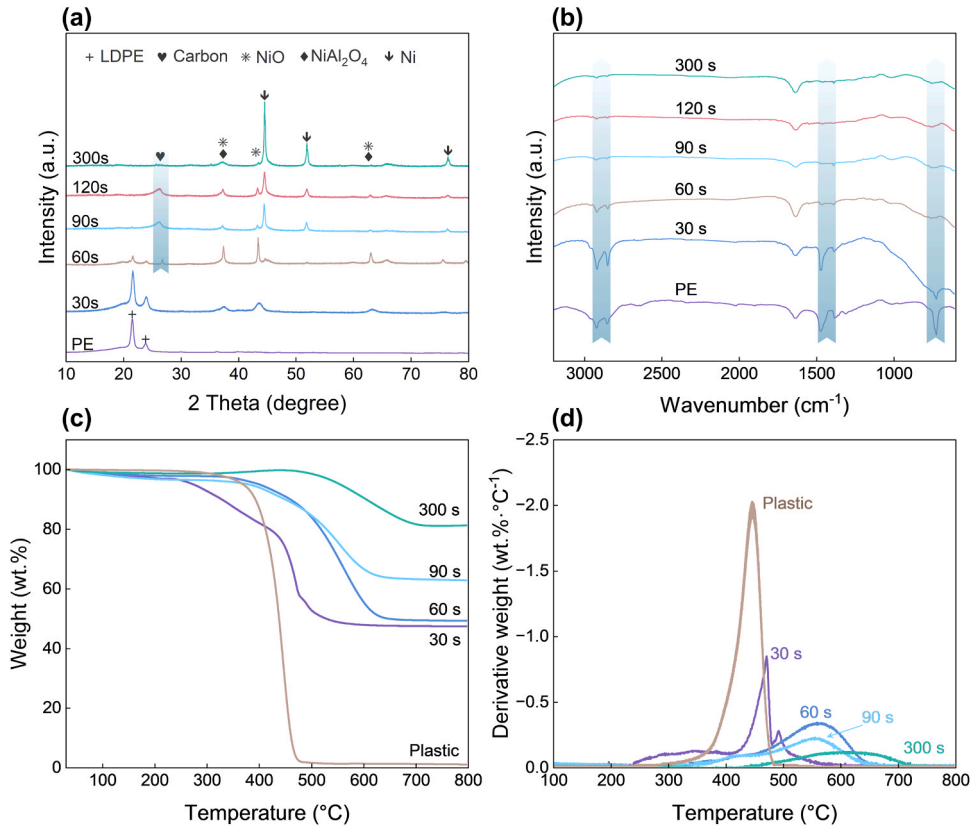

Fig. 7. Mimicked in-situ characterizations of mixed samples. The mixed samples were exposed to microwave irradiation for 30 s, 60 s, 90 s, 120 s, and 300 s (a) X-ray diffraction patterns; (b) FTIR spectra; (c) TG and (d) DTG analysis.

represented the electric or magnetic energy dissipation, while the imaginary part quantified the ability to convert absorbed energy into heat. The loss tangent of permittivity ($\tan\delta_\varepsilon = \varepsilon''/\varepsilon'$) and permeability ($\tan\delta_\mu = \mu''/\mu'$) were introduced to reflect the ability to convert electromagnetic energy into heat under microwave irradiation [52]. It should be mentioned that the microwave frequency of this reaction system was 2.45 GHz. Thus, the relevant results under 2.45 GHz were analyzed and shown in Fig. 4. As shown in Fig. 4a, the real part of complex permittivity was around 3.0 with slight fluctuation while the corresponding imaginary part was close to 0.35. Consequently, the loss tangent of permittivity for $LaNiO_x$, $MgNiO_x$, $CaNiO_x$ and $AlNiO_x$ was consistent around 0.12, indicating the obvious metal content-dependent relationship of Ni. Considering that basic metal oxides such as MgO and CaO were poor microwave absorbing materials [32], these four catalysts with the same Ni content might present close dielectric loss. It was also acknowledged that the magnetic loss originated from magnetic elements such as Fe, Ni and Co [53]. Therefore, the magnetic loss stayed around 0.3 with a modest variation. Generally, all the catalysts presented good microwave absorption performance and could initiate the reaction samples to the reaction temperature under microwave irradiation.

3.2. Optimization of reaction parameters

Plastic wastes could be decomposed into small molecular gas products through a thermo-chemical process and the high-throughput screen of catalysts further enhanced the generation of H_2 and CO. However, to obtain goal products of H_2 and CO other than CHs and solid carbon selectively and efficiently, the reaction condition including the reaction temperature, carrier gas and the reaction samples should be optimized. Specifically, key parameters such as microwave power, carrier gas composition and plastic/catalyst mass ratio had the combined effect on the valorization of plastic waste and CO_2 (Fig. 5). As shown in Fig. 5a, the H_2 yield increased from 298 mmol•$g^{-1}H_{plastic}$ to 415 mmol•$g^{-1}H_{plastic}$ by adjusting microwave power from 800 W to 1000 W under 50 vol% CO_2 concentration. This was due to the more rapid temperature gradient and higher terminal temperature with the increased microwave power (Fig. S9). A similar phenomenon has also been reported that extra energy input could avoid the byproducts by promoting the endothermic scission of the chemical C-H bond [24]. Correspondingly, the CH_4 yield slightly decreased from 28 mmol•$g^{-1}H_{plastic}$ to 11 mmol•$g^{-1}H_{plastic}$. It could be speculated that the generated CH_4 reacted with the CO_2 via a dry reforming reaction as confirmed by the tiny growth of H_2 yield along with the CO_2 concentration [40]. Contrary to the microwave power, adding more plastics into the reaction system posed a negative impact on the H_2 yield as the catalyst mass was controlled at 0.3 g. The H_2 yield was higher than 460 mmol•$g^{-1}H_{plastic}$, up to 92% of the theoretical value with fewer plastics (plastics/catalyst mass ratio = 0.5) due to the full contact between plastics and catalysts in the transient reaction process (Fig. 5d). As the plastics mass increased, part of the plastics which had no access to the catalysts would inevitably undergo the random C-C bond scission process driven by thermal convection, so that leading to the increment of small CHs [41]. This was consistent with the results in Fig. 5e that the CH_4 yield changed from 60 mmol•$g^{-1}H_{plastic}$ to 75 mmol•$g^{-1}H_{plastic}$ as the plastics/catalyst mass ratio increased from 0.5 to 2. Increasing CO_2 concentration alone had little influence on the H_2 yield at the moderated microwave power and plastics/catalyst mass ratio (Fig. 5a and g).

The introduction of CO_2 could change the carbon reallocation and promote the generation of CO instead of solid carbon. However, the activation of CO_2 required massive energy input at high temperatures for further participation in the reaction [42]. Meanwhile, the generation of CO was attributed to reforming between CO_2 and small chained CHs as well as the Boudouard reaction between CO_2 and solid carbon, and both reactions were endothermic. As shown in Fig. 5c, the carbon

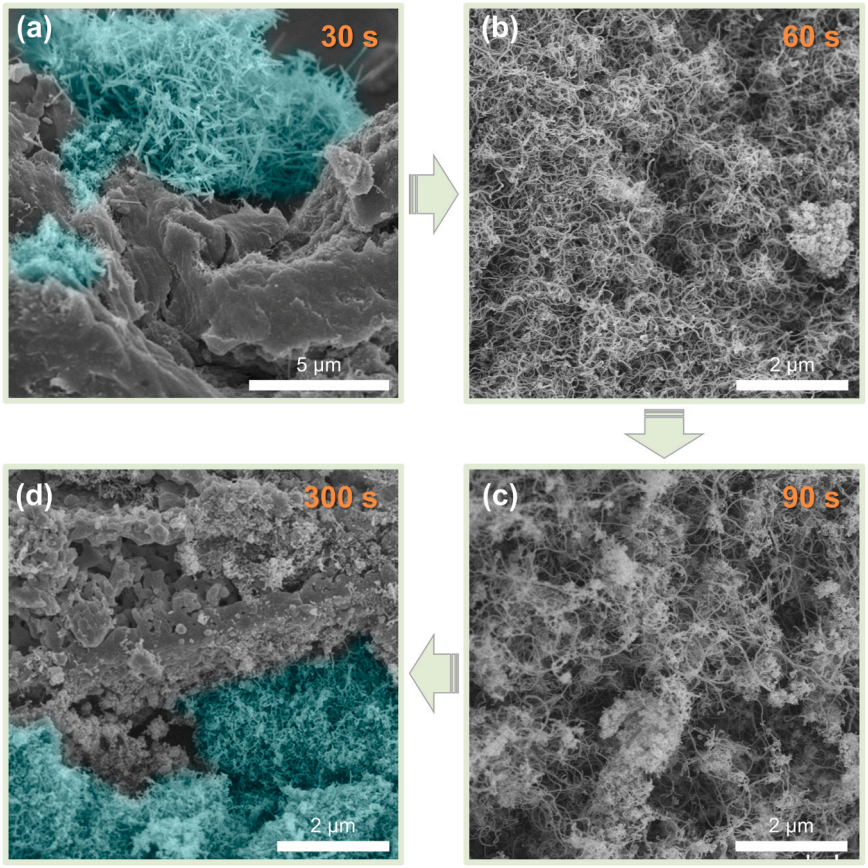

Fig. 8. SEM images of mixed samples on the time stream during the reaction process. The cyan color in (a) and (d) indicated the partial solid carbons. Apparent and dense solid carbons existed over the whole catalyst surface in (b) and (c) with no mark of cyan color.

conversion increased from 26% (microwave power = 800 W) to 48% (microwave power = 1000 W) with a CO_2 concentration of 50 vol% due to the direct temperature rise. Moreover, considering that both reactions needed the participation of CO_2, it seemed plausible that the increment of CO_2 concentration from 25% to 50% enhanced the carbon conversion (Fig. 5c and i). Nevertheless, it could also be observed that adding more CO_2 may not further enhance the generation of CO because of the slight decline trend. In terms of energy input, the amount of CO_2 that could be activated at a certain microwave power was limited and the extra CO_2 acted only as the carrier gas without participating in the reaction. Worse still, those inactivated CO_2 absorbed part of the energy which was to fulfill the activated gas, leading to the reduction of activated CO_2 gas. This reflected the combined impact of microwave power and CO_2 concentration to maximize carbon conversion. Similar to the trend of H_2 yield, a large plastics/catalyst mass ratio inhibited the carbon reallocation. On the one hand, more CHs would directly evolve out without reacting with activated CO_2 due to the random C-C scission of the excessive plastics. On the other hand, the decomposition of additional plastic feedstocks required more energy consumption, which accordingly hindered the CO_2 activation.

To sum up, tuning key parameters in the microwave-driven system could improve H_2 yield and carbon conversion significantly, and the combined effect should be taken into account. Boosting microwave power facilitated more energy input to accelerate plastic decomposition and CO_2 activation. A low plastics/catalyst mass ratio was beneficial for the complete catalytic valorization of plastics. However, given the modest variation in performance between the mass ratio of 0.5 and 1, adopting appropriate plastics might not only ensure high efficiency but also avoid overexpanding the catalysts. The introduction of CO_2 regulated the carbon evolution pathway effectively, whereas the excessive CO_2 would in turn impede the co-recycling process.

3.3. Time-on-stream analysis of decomposition process

To date, no experimental data was available to describe how CO_2 participated in the microwave-driven decomposition of plastic wastes. Therefore, the representative experiment on the time stream was conducted accompanied by the mimicked in-situ characterization (Figs. 6–8). Based on the optimization results in Section 3.2, 0.3 g PE sample and 0.3 g $AlNiO_x$ catalyst were mixed while the atmosphere was controlled at 50/50 vol% CO_2/N_2. Following exposure to the microwaves with the maximum power of 1000 W, the electromagnetic energy was preferentially absorbed by the $AlNiO_x$ catalysts other than the whole samples and transferred into heat rapidly. The temperature measured by the infrared pyrometer surged in the initial time of 56 s to over 620 °C with the average temperature gradient of 660 °C•min^{-1}, and subsequently dropped slightly to 550 °C (Fig. 6c). The inset figures taken from the infrared camera also demonstrated the same trend and showed the volumetric heating mode that the temperature spread out from the inside. As shown in Fig. 6a, H_2 began to evolve out within 20 s and rapidly increased to over 50 vol% among the generated gas products and the carrier gases in 80 s. From the onset of microwave irradiation, the dehydrogenation process was terminated in 300 s to 400 s, and the H_2 volume stopped at 413 ml after the sharp rise (Fig. 6b). Little CH_4 was detected with the volume of less than 30 ml, indicating the preferred dissociation of C-H bond. Unlike the evolution trend of H_2, CO was generated later in 50 s at the temperature of 600 °C. It has been mentioned that the CO_2 needed to be activated at a high temperature for further participation due to the poor reactivity [54]. Moreover, the temperature decreased to 550 °C due to the generation of CO, which also validated the activation of CO_2 as the high endothermic process. The generation of CO turned slow with the gas composition of less than 10 vol% from 450 s to 900 s. Such an ongoing and slow reaction process

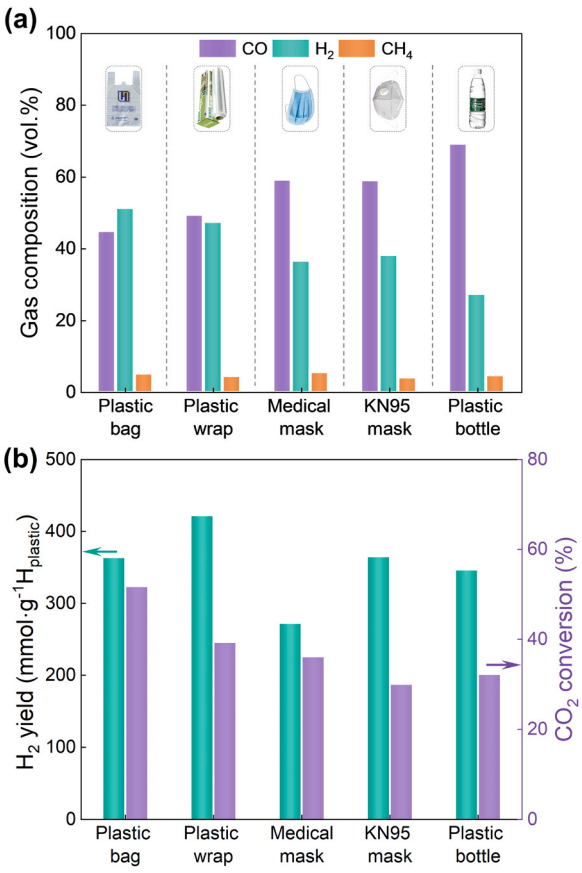

Fig. 9. Valorization of real-world plastic wastes. (a) Gas composition; (b) H_2 yield and CO_2 conversion.

was completely different from the decomposition of plastics and it might be speculated as the CO_2 reforming reaction with the residuals of plastic decomposition. As shown in Fig. 6b, the gas volume of CO reached 605 ml and kept expanding slightly. In general, the hydrogen in plastics was converted into H_2 with the H_2 yield of 467 mmol•g^{-1}H$_{plastic}$ (93.6% of the theoretical value). CO was generated with the carbon conversion of 62.1% and the CO_2 conversion of 41.3%.

Furthermore, mimicked in-situ characterizations have been carried out to reveal the evolution pathway of plastics and CO_2. In detail, the microwave reactor was stopped until the target time (30 s, 60 s, 90 s, 120 s and 300 s) and the samples were collected for analysis. Fresh catalysts from the same batch were employed for each experiment. The crystalline phases determined by X-ray diffraction were shown in Fig. 7a. With respect to the crystalline phase of nickel, the initial peak of NiO became weak and faded while the peak of Ni appeared and became sharp from 60 s to 300 s. The peaks of Ni at 44.5°, 51.8° and 76.4° were detected. This was ascribed to the in-situ reduction of NiO into metallic Ni with the generation of reductive H_2. The diffraction peaks of 21.6° and 23.9° assigned to the crystal plane (110) and (200) of PE faded in 60 s, demonstrating the dissociation of plastics and the presence of intermediate compounds. A serial reaction pathway was proposed by the thermal gravimetric analysis (Fig. 7c and d). In detail, PE was completely pyrolyzed under 500 °C and the DTG curve exhibited a narrow peak. Surprisingly, several peaks distinct from PE were detected and all shifted towards the higher temperature region. It could be revealed that part of the C-C bond was preferentially dissociated at a relatively low temperature, and PE was decomposed into intermediate compounds such as alkenes and solid residues. These compounds needed more energy for deconstruction at high temperatures. It has been reported that the presence of intermediates had limited influence on the efficient conversion of plastic in the microwave system [27]. Correspondingly, three sets of FTIR spectrum peaks belonging to PE have already become weak in the 60 s (Fig. 7b). In detail, the bands at 2920 cm^{-1} and 2848 cm^{-1} were assigned to CH_2 asymmetric stretching, and the peaks at 1470 cm^{-1} and 1376 cm^{-1} were assigned to the bending deformation as well as CH_3 symmetric deformation. The last peak at 717 cm^{-1} corresponded to the rocking deformation. As the reaction went on, the X-ray diffraction peak around 26° emerged from 60 s to 120 s and disappeared in 300 s dramatically, indicating the formation and consumption of solid carbons.

FESEM characterization of the samples collected on the time stream was employed to obtain direct insight into the change in morphologies over the catalysts. As shown in Fig. 8a, cluster-like carbon in short length marked in cyan was observed around the defect and interface of the catalysts in 30 s, confirming the dehydrogenation of plastics under low temperatures. Massive filamentous carbon and amorphous carbon were then facilitated and entirely covered the catalyst surface in 60 s (Fig. 8b). Similar results of solid carbon byproducts have been reported under N_2 atmosphere [22,35] and it seemed that the decomposition under CO_2 atmosphere followed the same pathway as catalytic pyrolysis under inert atmosphere, where plastics preferred to be decomposed into H_2 and solid carbons and CO_2 only acted as the carrier gas other than reactive gas. Nevertheless, the facilitated carbon products were distinctly reduced and the morphologies of carbon changed from dense to sparse, which coincided well with the generation of CO (Fig. 8c). With the dissolution of solid carbon, the catalyst surface was exposed with exsolved Ni nanoparticles (Fig. 8d). This was a highly original and valuable observation which displayed the evolution pathway of plastics and CO_2 through the combination of time-on-stream gas analysis and mimicked in-situ characterizations.

With respect to practical utilization, five kinds of representative plastic wastes in daily life were employed. The element analysis and FTIR characterization of these plastics (plastic bags, plastic wraps, medical masks, KN95 masks and plastic bottles) were shown in Table 1 and Fig. S11. According to statistics, polyethylene (medical masks and KN95 masks), polypropylene (plastic bags and plastic wraps) and polyethylene terephthalate (plastic bottles) accounted for over 60% of all plastic products in the world [31]. Moreover, such real-world plastic wastes contained various additives such as surface modifiers, material protectants and functionalizing agents [55], making the valorization even more challenging. Results showed that H_2 and CO were the dominant products (over 95 vol%) with little CH_4 for the five kinds of plastic wastes (Fig. 9a). The composition of H_2 and CO varied along with the element content of H and C in different plastic wastes. The highest H_2 yield was 412 mmol•g^{-1}H$_{plastic}$ for plastic bags while the CO_2 conversion exceeded 50% for plastic wraps (Fig. 9b). Generally, the novel microwave-driven valorization system proved the feasibility of tackling the real-world plastic wastes for high yield H_2 and CO.

3.4. Sustainability for microwave-driven valorization system

The successive cycle test over the $AlNiO_x$ catalyst was carried out to evaluate the stability for continuous running (Fig. 10). 0.3 g PE powder with no extra catalyst was added to the reaction system for each test. In terms of gas products, the H_2 rapidly evolved out in 20 s to 40 s followed by CO in 30 s to 60 s from the onset of the microwave. The cumulative volume of H_2 reached between 380 ml and 420 ml with no obvious decline for the cycle test. Meantime, the volume of CO kept over 450 ml with the highest value of 590 ml. From the gas composition in Fig. 10b, it could be concluded that H_2 and CO were the predominant gas products with little CH_4 of less than 5 vol%. Specifically, the H_2 yield for five-cycle test was 408 mmol•g^{-1}H$_{plastic}$, 480 mmol•g^{-1}H$_{plastic}$, 406 mmol•g^{-1}H$_{plastic}$, 410 mmol•g^{-1}H$_{plastic}$ and 437 mmol•g^{-1}H$_{plastic}$, respectively (Fig. 10c). This stable H_2 yield was extraordinarily different from the former results that H_2 yield would inevitably decrease due to the carbon deposition at N_2 atmosphere. Based on the element content, the theoretical H_2 yield was calculated as 500 mmol•g^{-1}H$_{plastic}$.

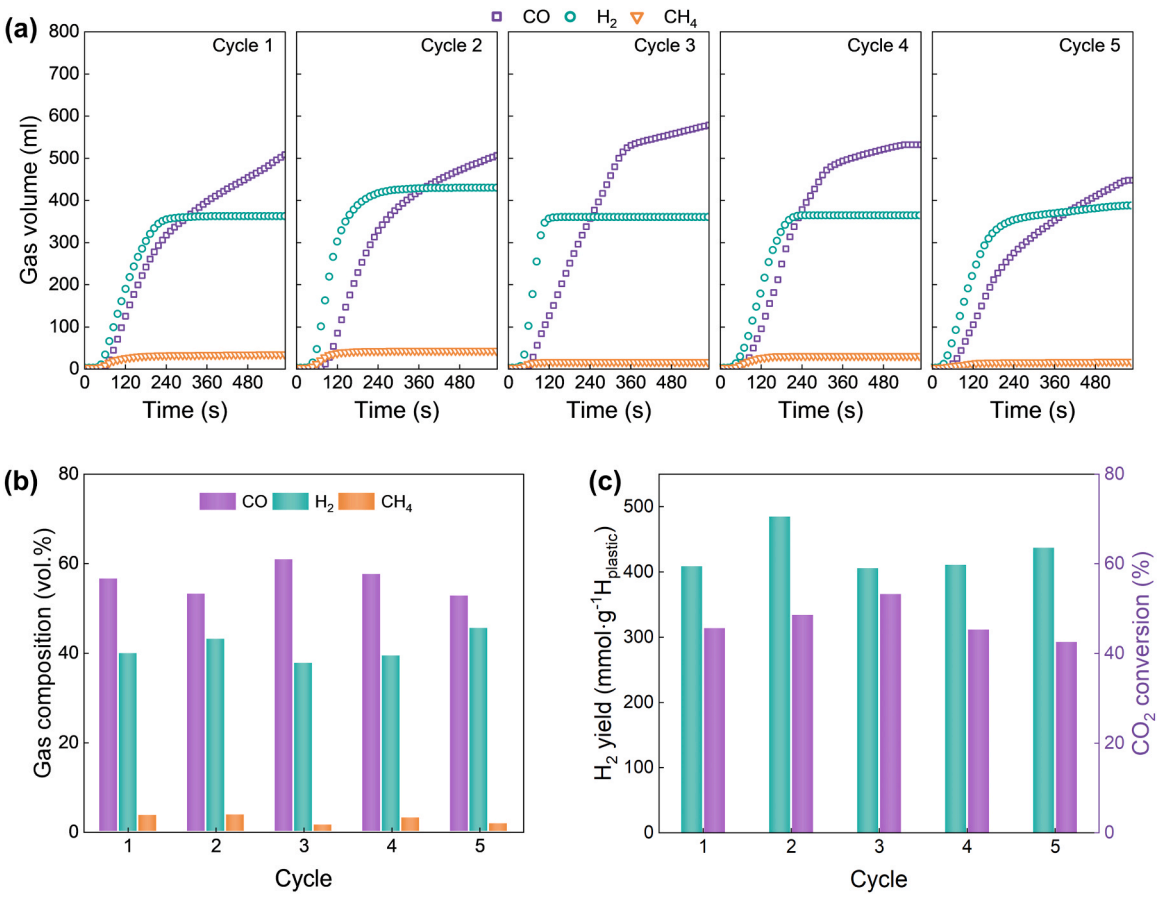

Fig. 10. Successive cycle test of microwave-driven valorization of plastic wastes and CO_2. (a) Gas volume of H_2, CO and CH_4; (b) Gas composition; (c) H_2 yield and CO_2 conversion.

Therefore, the highest H_2 yield in the second cycle was over 96% of theoretical value, manifesting the promising potential for pure H_2 generation. The CO_2 conversion maintained around 40%– 60%, manifesting the stable performance of eliminating solid carbon into CO. Generally, the integrated microwave-driven valorization of plastic waste and CO_2 over $NiAlO_x$ catalyst exhibited sustainable performance for high-yield H_2 and CO with no apparent decline in the successive cycle experiments.

The crystalline phases of spent catalysts were analyzed in Fig. 11a and the amplified XRD patterns in the range of $2\theta = 24° - 28°$ were shown in Fig. 11b. For the cycle test at CO_2 atmosphere, the peak with the strongest intensity was assigned to metallic Ni at 44.5° accompanied with peaks at 51.8° and 76.4°. Moreover, the peaks became a bit sharper with the cycle test, indicating a slight change in nanoparticle size. The crystallite size of metallic Ni was then calculated by Scherrer's equation according to the strongest peaks at 44.5° and the results were 24.99 nm, 27.19 nm, 34.92 nm, 27.31 nm and 37.37 nm. Consistent with the variation in peak intensity, the crystallite size of Ni exhibited a slight increment with the successive cycles. However, it was good to see that no sintering or agglomeration of nanoparticles happened which otherwise would lead to severe catalyst deactivation. The presence of the broad peak around 26° represented the deposition of solid carbon over the catalyst surface. Compared with the results at N_2 atmosphere, the intensity of peaks for the five-cycle test at CO_2 atmosphere was relatively low, indicating the stable removal performance of solid carbon. This could also be confirmed by the Roman spectrum as well as the TG analysis (Fig. 11 c and d). As shown in Fig. 11c, two strong peaks at 1346 cm^{-1} and 1588 cm^{-1} were detected for the spent catalysts at N_2 atmosphere, which was an indication of carbon deposition. In detail, the D band at 1346 cm^{-1} was induced by the structural disorder of carbon materials while the G band at 1588 cm^{-1} corresponded to the in-plane stretching of graphite C-C bonds [56]. By contrast, the intensity of these two peaks in the cycle test at CO_2 atmosphere were all negligible. This again demonstrated the positive role of CO_2 for stable performance by eliminating carbon materials. The TG profiles provided quantified results of the carbon residues (Fig. 11d). The common mass increase at the low-temperature range was the oxidation of metallic nickel to form nickel oxides and the mass decrease at the high temperature indicated the oxidation of deposited carbons to form carbon monoxide or carbon dioxide. Thus, the real mass decrease was calculated as the maximum value minus the final value. The spent catalysts at N_2 atmosphere showed a mass loss of 24.5 wt%. By contrast, the spent catalysts at CO_2 atmosphere after the first cycle, third cycle and fifth cycle contained carbon residues of 3.2 wt%, 3.6 wt% and 6.2 wt%, respectively.

3.5. *Mechanism of microwave-driven CO_2 gasification of plastic waste*

Based on the findings above, the potential mechanism of microwave-driven valorization of plastic wastes and CO_2 was proposed for the first time as shown in Fig. 12. The thermal effect and plasma effect of microwave-material interaction facilitated the valorization of plastic wastes and CO_2. Due to the selective heating of microwaves, the temperature of $AlNiO_x$ catalysts increased sharply to over 600 °C within 60 s, while the plastics, insensitive to microwaves, remained minimally heated (Fig. 12d). The huge temperature gap between catalysts and plastics could help promote and intensify the simultaneous heat and mass transfer. Furthermore, due to the close distribution of catalyst nanoparticles, the local electric field distortion occurred and caused enhanced electromagnetic dissipation (Fig. 12e). The plasma discharging was then induced due to the excessive electric field distortion and

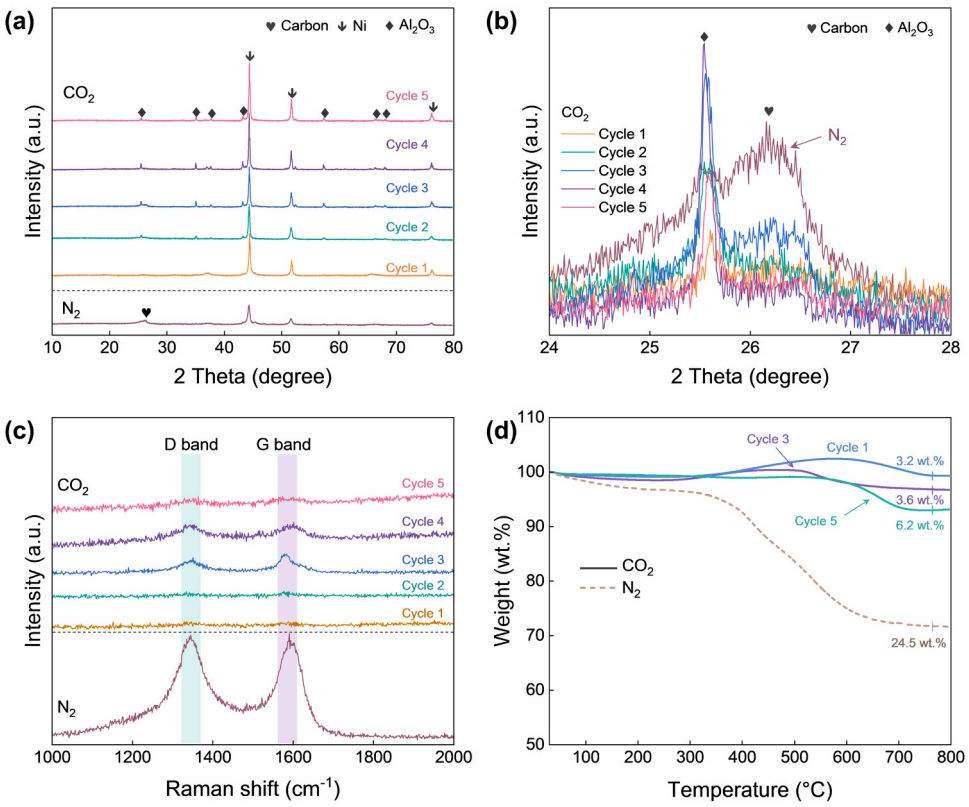

Fig. 11. Characterization of spent catalysts for successive tests. (a, b) X-ray diffraction patterns; (c) Raman spectra; (d) TG analysis.

interfacial polarization, breaking through the surrounding medium accompanied by huge energy and free radicals (Fig. S12). The collision frequency and intensity between the reactants in the plasma region were thereby reinforced. The combined thermal-plasma effect facilitated the efficient microwave-driven recycling of plastic wastes in contrast to the conventional thermal-driven process.

The pathway of microwave-driven CO_2 gasification of plastic wastes was shown in Fig. 12a. From the onset of microwave irradiation, the electromagnetic energy was absorbed intensely by the $AlNiO_x$ catalysts and transferred into heat as the driving force of reactions. The dehydrogenation of plastics occurred and C-H bond selective scission took place due to the rapid activation of catalysts. Massive H_2 was generated and solid carbon residues began to deposit over the catalyst surface. By-products from the random scission due to the slight heating rate could be avoided. As the temperature increased, CO_2 was subsequently activated and participated in the reaction via CO_2 gasification. The Boudouard reaction between solid carbon residues and activated CO_2 was initiated. Former studies have reported that the Boudouard reaction was extremely endothermic and the free energy became positive until the temperature was over 700 °C [37,57]. In the conventional thermal process, even a 4-fold enhancement of carbon conversion was achieved by increasing the reaction temperature from 500 °C to 700 °C, the carbon conversion (<10%) and CO_2 conversion (<1%) were far from efficient (Fig. 13b). Nevertheless, the carbon conversion exceeded over 60% with a 6.5-fold enhancement while CO_2 conversion increased to 41.3% under microwave irradiation. The selective heating of carbon under microwave resulted in the changed thermodynamics with dropped apparent activation energy, favorable for the more facile generation of CO. It has been presumed that the microwave-specific enhanced reactivity originated from the interaction of CO_2 with the steady-state concentration of electron-hole pairs presented at the carbon surface due to the space-charge mechanism [37]. Additional experimental data was provided for the microwave-specific boosting of the Boudouard reaction in Figs. S13 and S14. In addition, the slight increase in H_2 yield with the introduction of CO_2 also suggested the initiation of the dry reforming reaction (Fig. 13a).

To demonstrate the sustainability, the TEM characterizations of the fresh and spent $AlNiO_x$ catalysts were performed as shown in Fig. 12b and c. The in-situ reduction took place with the generated H_2 and metallic nickel exsolved out from the crystal lattice to the surface. The nickel element was distributed uniformly among the substrate of metal oxides for the fresh $AlNiO_x$ catalysts. It has already been reported that the embedded nanoparticles were unfavorable for the catalytic activity due to the limited contact with the reactants [58]. An obvious morphology change occurred during the decomposition process, and the nickel nanoparticles were exsolved from the substrate and formed the anchored structure [59]. This anchoring effect was believed to provide enhanced thermal stability by preventing severe agglomeration. Moreover, microwave absorptivity for the spent catalysts was evaluated in Fig. 12f. Compared with the fresh catalyst, both the real part and imaginary part of the permittivity increased dramatically, and the dielectric loss exhibited a 5.3-fold enhancement. This was attributed to the deposited carbons which was excellent microwave absorber. On the other hand, results showed that the majority of deposited carbon (> 93 wt%) over the catalyst surface was eliminated and converted into CO, leaving a minor amount of carbon residues. The excellent stability of the successive cycle test demonstrated that those carbon residues had a limited effect on the catalytic performance. Besides, the enhanced microwave absorptivity due to the carbon residues would in turn make the next decomposition process more rapid and efficient.

4. Conclusions

In this work, we have proposed a microwave-driven system for sustainable and efficient valorization of plastic wastes and CO_2 for high-yield H_2 (96% of theoretical value) and CO. The results for the high-throughput screen of metal oxide catalysts demonstrated that effective microwave catalysts should be reducible for in-situ exsolution of

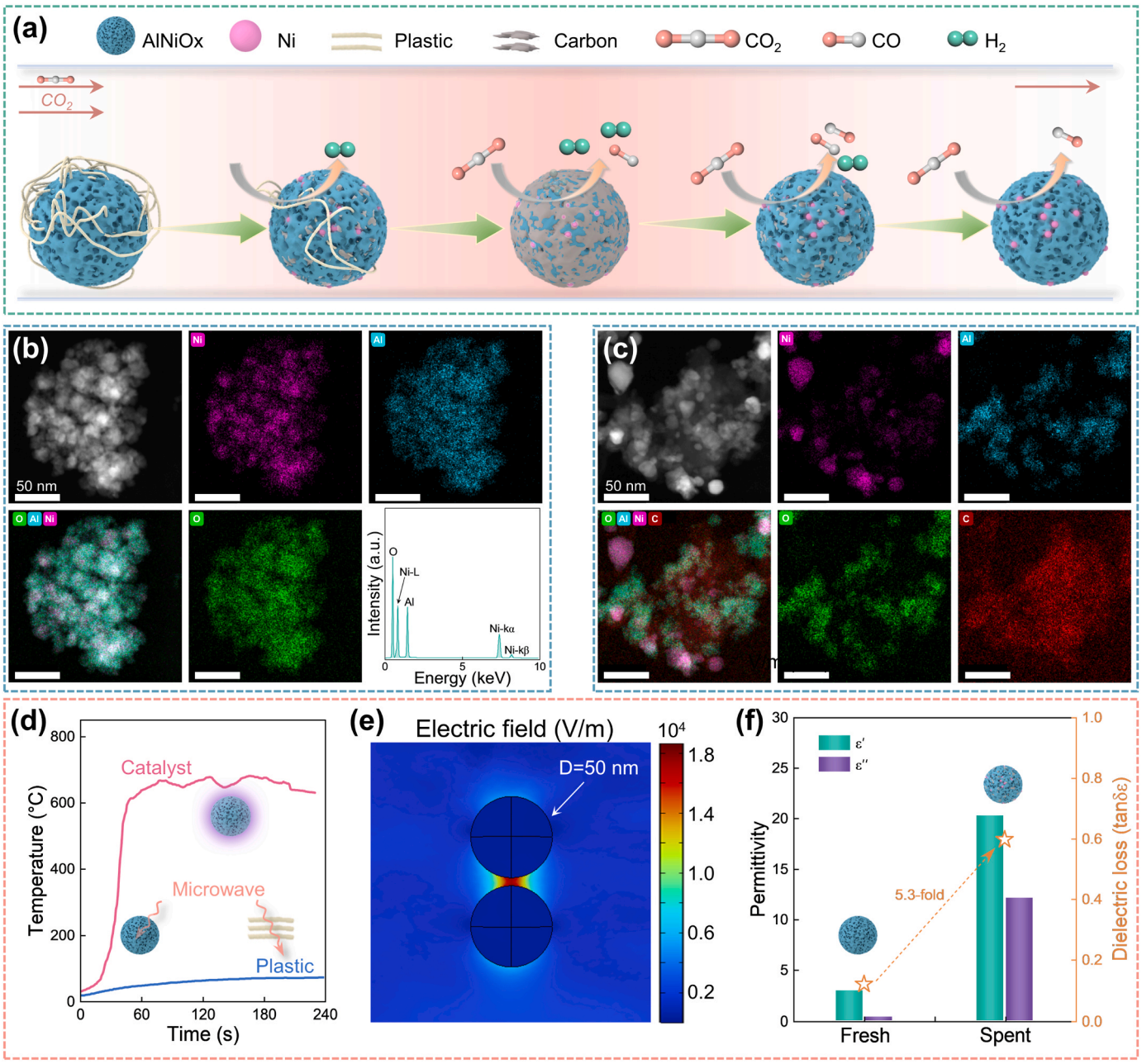

Fig. 12. Proposed mechanism. (a) Illustration on the microwave-driven CO_2 gasification of plastic wastes; HAADF image and corresponding elemental mapping images of (b) fresh $AlNiO_x$ and (c) spent $AlNiO_x$; (d) Temperature gradient between catalysts and plastics; (e)Electric field between catalyst particles; (f) Electromagnetic parameters of fresh and spent $AlNiO_x$ catalyst.

metallic nanoparticles, and $AlNiO_x$ catalyst exhibited the best performance of H_2 yield (~480 mmol•$g^{-1}H_{plastic}$), carbon conversion (~70%) and CO_2 conversion (~53%). Key parameters of the microwave-driven system were tuned and the combined effect was taken into account via response surface analysis. Results showed that boosting microwave power to 1000 W facilitated more energy input to accelerate plastic decomposition and CO_2 activation. The appropriate plastics/catalyst mass ratio of 1:1 could not only ensure high efficiency but also avoid overexpanding the catalysts. Noteworthy, the introduction of CO_2 regulated the carbon evolution pathway effectively, whereas the excessive CO_2 would in turn impede the co-recycling process. Plastic wastes were mainly decomposed into H_2 and solid carbon residues under microwave irradiation. With the increase in the temperature, the deposited carbons were eliminated by reacting with the activated CO_2 gas to generate CO via CO_2 gasification. Therefore, the sustainability and stability of high-yield H_2 generation were achieved for successive cycle tests. In addition, this integrated method was successfully employed to recycle five typical plastic wastes in daily life and demonstrated the potential for practical applications. In all, the microwave-driven CO_2 gasification system provided an efficient and sustainable alternative to convert plastic wastes into H_2 and CO, which benefited the waste-to-energy circular economy.

CRediT authorship contribution statement

Liang Cai: Writing – review & editing, Supervision, Funding acquisition, Conceptualization. **Zhang Peng:** Writing – review & editing, Writing – original draft, Methodology, Investigation, Formal analysis, Conceptualization. **Chen Xiaoping:** Writing – review & editing, Visualization. **Li Yongjie:** Validation, Investigation. **Ma Jiliang:** Writing –

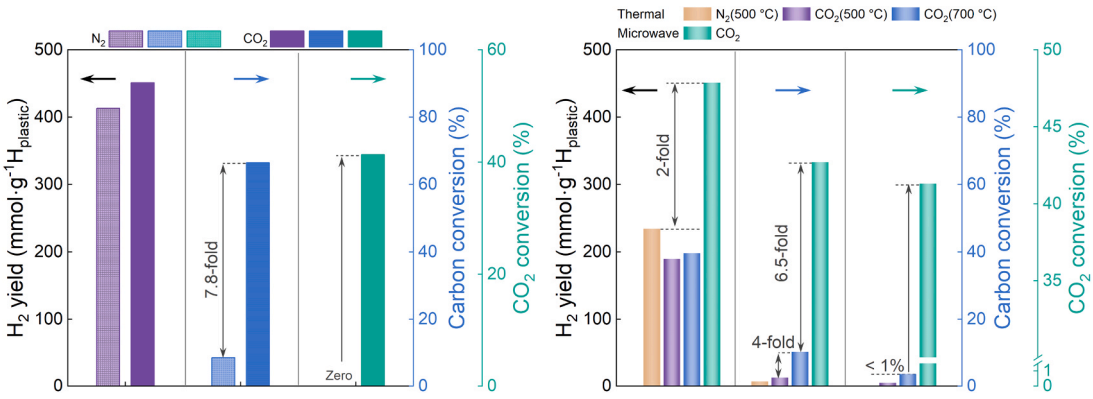

Fig. 13. Comparison of H_2 yield, carbon conversion and CO_2 conversion for the valorization of 0.3 g plastic wastes using 0.3 g $AlNiO_x$ catalyst between (a) N_2 atmosphere and CO_2 atmosphere under microwave-driven process; (b) thermal-driven and microwave-driven process.

review & editing. **Liu Daoyin:** Writing – review & editing. **Wu Mudi:** Writing – review & editing, Supervision, Conceptualization.

Declaration of Competing Interest

The authors declare that they have no known competing financial interests or personal relationships that could have appeared to influence the work reported in this paper.

Data availability

Data will be made available on request.

Appendix A. Supporting information

Supplementary data associated with this article can be found in the online version at doi:10.1016/j.apcatb.2024.123718.

References

[1] K. Lee, Y. Jing, Y. Wang, N. Yan, A unified view on catalytic conversion of biomass and waste plastics, Nat. Rev. Chem. 6 (2022) 635–652.
[2] L. Dai, N. Zhou, Y. Lv, Y. Cheng, Y. Wang, Y. Liu, K. Cobb, P. Chen, H. Lei, R. Ruan, Pyrolysis technology for plastic waste recycling: A state-of-the-art review, Prog. Energy Combust. Sci. 93 (2022) 101021.
[3] P. Stegmann, V. Daioglou, M. Londo, D.P. van Vuuren, M. Junginger, Plastic futures and their CO_2 emissions, Nature 612 (2022) 272–276.
[4] S.M. Al-Salem, P. Lettieri, J. Baeyens, The valorization of plastic solid waste (PSW) by primary to quaternary routes: From re-use to energy and chemicals, Prog. Energy Combust. Sci. 36 (2010) 103–129.
[5] K. Zheng, Y. Wu, Z. Hu, S. Wang, X. Jiao, J. Zhu, Y. Sun, Y. Xie, Progress and perspective for conversion of plastic wastes into valuable chemicals, Chem. Soc. Rev. 52 (2022) 8–29.
[6] B.M. Weckhuysen, Creating value from plastic waste, Science 370 (2020) 400–401.
[7] Q. Zhu, H. Zhou, L. Wang, L. Wang, C. Wang, H. Wang, W. Fang, M. He, Q. Wu, F. S. Xiao, Enhanced CO_2 utilization in dry reforming of methane achieved through nickel-mediated hydrogen spillover in zeolite crystals, Nat. Catal. 5 (2022) 1030–1037.
[8] G. Wen, B. Ren, X. Wang, D. Luo, H. Dou, Y. Zheng, R. Gao, J. Gostick, A. Yu, Z. Chen, Continuous CO_2 electrolysis using a CO_2 exsolution-induced flow cell, Nat. Energy 7 (2022) 978–988.
[9] H. Xin, L. Lin, R. Li, D. Li, T. Song, R. Mu, Q. Fu, X. Bao, Overturning CO_2 hydrogenation selectivity with high activity via reaction-induced strong metal-support interactions, J. Am. Chem. Soc. 144 (2022) 4874–4882.
[10] S. Bhattacharjee, M. Rahaman, V. Andrei, M. Miller, S. Rodríguez-Jiménez, E. Lam, C. Pornrungroj, E. Reisner, Photoelectrochemical CO_2-to-fuel conversion with simultaneous plastic reforming, Nat. Synth. 2 (2023) 182–192.
[11] J. Wang, X. Li, M. Wang, T. Zhang, X. Chai, J. Lu, T. Wang, Y. Zhao, D. Ma, Electrocatalytic valorization of poly(ethylene terephthalate) plastic and CO_2 for simultaneous production of formic acid, ACS Catal. 12 (2022) 6722–6728.
[12] S.L. Wu, J.H. Kuo, M.Y. Wey, Design of catalysts comprising a nickel core and ceria shell for hydrogen production from plastic waste gasification: An integrated test for anti-coking and catalytic performance, Catal. Sci. Technol. 10 (2020) 3975–3984.
[13] J. Wang, Y. Pan, J. Song, Q. Huang, A high-quality hydrogen production strategy from waste plastics through microwave-assisted reactions with heterogeneous bimetallic iron/nickel/cerium catalysts, J. Anal. Appl. Pyrolysis 166 (2022) 105612.
[14] D.V. Suriapparao, T.H. Kumar, B.R. Reddy, A. Yerrayya, B.A. Srinivas, P. Sivakumar, S.R. Prakash, C.S. Rao, V. Sridevi, J. Desinghu, Role of ZSM5 catalyst and char susceptor on the synthesis of chemicals and hydrocarbons from microwave-assisted in-situ catalytic co-pyrolysis of algae and plastic wastes, Renew. Energy 181 (2022) 990–999.
[15] K. Ding, S. Liu, Y. Huang, S. Liu, N. Zhou, P. Peng, Y. Wang, P. Chen, R. Ruan, Catalytic microwave-assisted pyrolysis of plastic waste over NiO and HY for gasoline-range hydrocarbons production, Energy Conv. Manag. 196 (2019) 1316–1325.
[16] Q. Hu, Y.S. Ok, C.H. Wang, Sustainable and highly efficient recycling of plastic waste into syngas via a chemical looping scheme, Environ. Sci. Technol. 56 (2022) 8953–8963.
[17] S. Zhang, S. Zhu, H. Zhang, X. Liu, Y. Xiong, High quality H_2-rich syngas production from pyrolysis-gasification of biomass and plastic wastes by Ni-Fe@ Nanofibers/Porous carbon catalyst, Int. J. Hydrog. Energy 44 (2019) 26193–26203.
[18] X. Shen, Z. Zhao, H. Li, X. Gao, X. Fan, Microwave-assisted pyrolysis of plastics with iron-based catalysts for hydrogen and carbon nanotubes production, Mater. Today Chem. 26 (2022) 101166.
[19] X. Yuan, N.M. Kumar, B. Brigljevic, S. Li, S. Deng, M. Byun, B. Lee, C.S.K. Lin, D.C. W. Tsang, K.B. Lee, S.S. Chopra, H. Lim, Y.S. Ok, Sustainability-inspired upcycling of waste polyethylene terephthalate plastic into porous carbon for CO_2 capture, Green. Chem. 24 (2022) 1494–1504.
[20] D. Yao, H. Li, Y. Dai, C.H. Wang, Impact of temperature on the activity of Fe-Ni catalysts for pyrolysis and decomposition processing of plastic waste, Chem. Eng. J. 408 (2021) 127268.
[21] D. Yao, H. Yang, H. Chen, P.T. Williams, Co-precipitation, impregnation and so-gel preparation of Ni catalysts for pyrolysis-catalytic steam reforming of waste plastics, Appl. Catal. B: Environ. 239 (2018) 565–577.
[22] W. Li, K. Qian, Z. Yang, X. Ding, W. Tian, D. Chen, Promotion effect of cobalt doping on microwave-initiated plastic deconstruction for hydrogen production over iron catalysts, Appl. Catal. B: Environ. 327 (2023) 122451.
[23] C. Wu, M.A. Nahil, N. Miskolczi, J. Huang, P.T. Williams, Processing real-world waste plastics by pyrolysis-reforming for hydrogen and high-value carbon nanotubes, Environ. Sci. Technol. 48 (2014) 819–826.
[24] D. Yao, Y. Zhang, P.T. Williams, H. Yang, H. Chen, Co-production of hydrogen and carbon nanotubes from real-world waste plastics: Influence of catalyst composition and operational parameters, Appl. Catal. B: Environ. 221 (2018) 584–597.
[25] Y. Zhang, P.T. Williams, Carbon nanotubes and hydrogen production from the pyrolysis catalysis or catalytic-steam reforming of waste tyres, J. Anal. Appl. Pyrolysis 122 (2016) 490–501.
[26] T. Uekert, M.F. Kuehnel, D.W. Wakerley, E. Reisner, Plastic waste as a feedstock for solar-driven H_2 generation, Energy Environ. Sci. 11 (2018) 2853–2857.
[27] X. Jie, W. Li, D. Slocombe, Y. Gao, I. Banerjee, S. Gonzalez-Cortes, B. Yao, H. AlMegren, S. Alshihri, J. Dilworth, J. Thomas, T. Xiao, P. Edwards, Microwave-initiated catalytic deconstruction of plastic waste into hydrogen and high-value carbons, Nat. Catal. 3 (2020) 902–912.
[28] K.M. Wyss, K.J. Silva, K.V. Bets, W.A. Algozeeb, C. Kittrell, C.H. Teng, C.H. Choi, W. Chen, J.L. Beckham, B.I. Yakobson, J.M. Tour, Synthesis of clean hydrogen gas from waste plastic at zero net cost, Adv. Mater. (2023) 2306763.
[29] X. Jie, S. Gonzalez-Cortes, T. Xiao, B. Yao, J. Wang, D.R. Slocombe, Y. Fang, N. Miller, H.A. Al-Megren, J.R. Dilworth, J.M. Thomas, P.P. Edwards, The decarbonisation of petroleum and other fossil hydrocarbon fuels for the facile production and safe storage of hydrogen, Energy Environ. Sci. 12 (2019) 238–249.
[30] Q. Cao, H.C. Dai, J.H. He, C.L. Wang, C. Zhou, X.F. Cheng, J.M. Lu, Microwave-initiated MAX Ti_3AlC_2-catalyzed upcycling of polyolefin plastic wastes: Selective conversion to hydrogen and carbon nanofibers for sodium-ion battery, Appl. Catal. B: Environ. 318 (2022) 121828.
[31] P.H.M. Putra, S. Rozali, M.F. Abdul Patah, A. Idris, A review of microwave pyrolysis as a sustainable plastic waste management technique, J. Environ. Manag. 303 (2022) 114240.
[32] C.M. Marin, E.J. Popczun, T.D. Nguyen-Phan, D.N. Tafen, D. Alfonso, I. Waluyo, A. Hunt, D.R. Kauffman, Designing perovskite catalysts for controlled active-site

exsolution in the microwave dry reforming of methane, Appl. Catal. B: Environ. 284 (2021) 119711.
[33] J. Chen, W. Xu, J. Zhu, X. Wang, J. Zhou, Highly effective direct decomposition of H2S by microwave catalysis on core-shell Mo2N-MoC@SiO2 microwave catalyst, Appl. Catal. B: Environ. 268 (2020) 118454.
[34] J. Jia, A. Veksha, T.T. Lim, G. Lisak, Weakening the strong Fe-La interaction in A-site-deficient perovskite via Ni substitution to promote the thermocatalytic synthesis of carbon nanotubes from plastics, J. Hazard. Mater. 403 (2021) 123642.
[35] D. Yao, H. Li, B.C. Mohan, A.K. Prabhakar, Y. Dai, C.H. Wang, Conversion of waste plastic packings to carbon nanomaterials: Investigation into catalyst material, waste type, and product applications, ACS Sustain, Chem. Eng. 10 (2022) 1125–1136.
[36] K.P. Gopinath, V.M. Nagarajan, A. Krishnan, R. Malolan, A critical review on the influence of energy, environmental and economic factors on various processes used to handle and recycle plastic wastes: Development of a comprehensive index, J. Clean. Prod. 274 (2020) 123031.
[37] J. Hunt, A. Ferrari, A. Lita, M. Crosswhite, B. Ashley, A.E. Stiegman, Microwave-specific enhancement of the carbon-carbon dioxide (Boudouard) reaction, J. Phys. Chem. C. 117 (2013) 26871–26880.
[38] M. Kosari, S. Askari, A.M. Seayad, S. Xi, S. Kawi, A. Borgna, H.C. Zeng, Strong coke-resistivity of spherical hollow Ni/SiO2 catalysts with shell-confined high-content Ni nanoparticles for methane dry reforming with CO2, Appl. Catal. B: Environ. 310 (2022) 121360.
[39] J. Lin, R. Ma, J. Luo, S. Sun, C. Cui, L. Fang, H. Huang, Microwave pyrolysis of food waste for high-quality syngas production: Positive effects of a CO_2 reaction atmosphere and insights into the intrinsic reaction mechanisms, Energy Conv, Manag 206 (2020) 112490.
[40] J. Lin, C. Cui, S. Sun, D. Xu, R. Ma, M. Wang, L. Fang, B. Dong, Enhanced combined H_2O/CO_2 reforming of sludge to produce high-quality syngas via spiral continuous microwave pyrolysis technology: CO_2 reforming mechanism and H_2/CO directional regulation, Chem. Eng. J. 434 (2022) 134628.
[41] S. Jung, Y.F. Tsang, D. Kwon, D. Choi, W.H. Chen, Y.H. Kim, D.H. Moon, E. E. Kwon, CO_2-mediated thermal treatment of disposable plastic food containers, Chem. Eng. J. 451 (2023) 138603.
[42] D. Kwon, S. Jung, D.H. Moon, Y.F. Tsang, W.H. Chen, E.E. Kwon, Strategic management of harmful chemicals produced from pyrolysis of plastic cup waste using CO_2 as a reaction medium, Chem. Eng. J. 437 (2022) 135524.
[43] D. Choi, S. Jung, Y.F. Tsang, H. Song, D.H. Moon, E.E. Kwon, Sustainable valorization of styrofoam and CO_2 into syngas, Sci. Total Environ. 834 (2022) 155384.
[44] S. Jung, J.H. Kim, Y.F. Tsang, H. Song, E.E. Kwon, Valorizing plastic toy wastes to flammable gases through CO_2-mediated pyrolysis with a Co-based, Catal., J. Hazard. Mater. 434 (2022) 128850.
[45] Y.N. Chun, H.G. Song, Microwave-induced carbon-CO_2 gasification for energy conversion, Energy 190 (2020) 116386.
[46] P. Lahijani, Z.A. Zainal, A.R. Mohamed, M. Mohammadi, Microwave-enhanced CO_2 gasification of oil palm shell char, Bioresour. Technol. 158 (2014) 193–200.
[47] J. Luo, C. Cui, S. Sun, Z. Hu, R. Ma, M. Wang, J. Lin, Leveraging CO_2 to directionally control the H_2/CO ratio in continuous microwave pyrolysis/gasification of waste plastics: Quantitative analysis of CO_2 and density functional theory calculations of regulation mechanism, Chem. Eng. J. 435 (2022) 134794.
[48] J. Jia, A. Veksha, T.T. Lim, G. Lisak, In situ grown metallic nickel from X-Ni (X=La, Mg, Sr) oxides for converting plastics into carbon nanotubes: Influence of metal-support interaction, J. Clean. Prod. 258 (2020) 120633.
[49] Y. Yang, J. Li, Y. Sun, The metal/oxide heterointerface delivered by solid-based exsolution strategy: A review, Chem. Eng. J. 440 (2022) 135868.
[50] S. Glowniak, B. Szczesniak, J. Choma, M. Jaroniec, Advances in microwave synthesis of nanoporous materials, Adv. Mater. 33 (2021) 2103477.
[51] J. Bakerjarvis, E.J. Vanzura, W.A. Kissick, Improved technique for determining complex permittivity with the transmission reflection method, IEEE Trans. Microw. Theory Tech. 38 (1990) 1096–1103.
[52] T.Y. Chen, M. Baker-Fales, H. Goyal, D.G. Vlachos, Microwave heating-induced temperature gradients in liquid-liquid biphasic systems, Ind. Eng. Chem. Res. 61 (2022) 3011–3022.
[53] X. Di, Y. Wang, Y. Fu, X. Wu, P. Wang, Wheat flour-derived nanoporous carbon@$ZnFe_2O_4$ hierarchical composite as an outstanding microwave absorber, Carbon 173 (2021) 174–184.
[54] Y. Kim, J.I. Oh, M. Vithanage, Y.K. Park, J. Lee, E.E. Kwon, Modification of biochar properties using CO_2, Chem. Eng. J. 372 (2019) 383–389.
[55] A. Barrick, O. Champeau, A. Chatel, N. Manier, G. Northcott, L.A. Tremblay, Plastic additives: challenges in ecotox hazard assessment, PeerJ 9 (2021) 11300.
[56] J. Huang, A. Veksha, T. Jun, G. Lisak, Upgrading waste plastic derived pyrolysis gas via chemical looping cracking-gasification using Ni-Fe-Al redox catalysts, Chem. Eng. J. 438 (2022) 135580.
[57] R. Davì, G. Carraro, M. Stojkovska, M. Smerieri, L. Savio, M. Lewandowski, J. J. Gallet, F. Bournel, M. Rocca, L. Vattuone, Boudouard reaction under graphene cover on Ni(111), Appl. Surf. Sci. 599 (2022) 154065.
[58] T. Zhu, H.E. Troiani, L.V. Mogni, M. Han, S.A. Barnett, Ni-substituted $Sr(Ti,Fe)O_3$ SOFC anodes: Achieving high performance via metal alloy nanoparticle exsolution, Joule 2 (2018) 478–496.
[59] H. Lv, L. Lin, X. Zhang, Y. Song, H. Matsumoto, C. Zeng, N. Ta, W. Liu, D. Gao, G. Wang, X. Bao, In situ investigation of reversible exsolution/dissolution of CoFe alloy nanoparticles in a Co-doped $Sr_2Fe_{1.5}Mo_{0.5}O_{6\text{-delta}}$ cathode for CO_2 electrolysis, Adv. Mater. 32 (2020) 1906193.